01 Aug 2019

Computational Study of the Ro-Vibrational Spectrum of CO-CO₂

Eduardo Castro-Juarez

Xiao-Gang Wang

Tucker Carrington Jr.

Ernesto Quintas-Sánchez
Missouri University of Science and Technology, quintassancheze@mst.edu

et. al. For a complete list of authors, see *https://scholarsmine.mst.edu/chem_facwork/2984*

Recommended Citation

Computational study of the ro-vibrational spectrum of CO–CO$_2$

View Online   Export Citation   CrossMark

Eduardo Castro-Juárez,[1] [ID] Xiao-Gang Wang,[1] [ID] Tucker Carrington, Jr.,[1,a) [ID] Ernesto Quintas-Sánchez,[2] [ID] and Richard Dawes[2] [ID]

AFFILIATIONS

[1] Chemistry Department, Queen's University, Kingston, Ontario K7L 3N6, Canada
[2] Department of Chemistry, Missouri University of Science and Technology, Rolla, Missouri 65409, USA

a) Electronic mail: Tucker.Carrington@queensu.ca

ABSTRACT

An accurate *ab initio* ground-state intermolecular potential energy surface (PES) was determined for the CO–CO$_2$ van der Waals dimer. The Lanczos algorithm was used to compute rovibrational energies on this PES. For both the C-in and O-in T-shaped isomers, the fundamental transition frequencies agree well with previous experimental results. We confirm that the in-plane states previously observed are geared states. In addition, we have computed and assigned many other vibrational states. The rotational constants we determine from $J = 1$ energy levels agree well with their experimental counterparts. Planar and out-of-plane cuts of some of the wavefunctions we compute are quite different, indicating strong coupling between the bend and torsional modes. Because the stable isomers are T-shaped, vibration along the out-of-plane coordinates is very floppy. In CO–CO$_2$, when the molecule is out-of-plane, interconversion of the isomers is possible, but the barrier height is higher than the in-plane geared barrier height.

Published under license by AIP Publishing. https://doi.org/10.1063/1.5119762

I. INTRODUCTION

CO–CO$_2$ is a van der Waals dimer composed of the two monomers CO and CO$_2$, both of which are of astrophysical interest. Its infrared and microwave spectra have been recorded and its structure determined.[1–3] CO–CO$_2$ has two stable isomers. Both are T-shaped with the CO$_2$ monomer at the top of the T and the CO monomer at the stem of the T. The lower-energy isomer has the C of CO close to the C of CO$_2$. The higher-energy isomer has the O of CO close to the C of CO$_2$. We shall refer to these isomers as C-in and O-in. Both isomers are shown on the right side of Fig. 1. The C-in isomer was first studied by Legon and Suckley[1] and later by others.[4,5] The existence of the O-in isomer was predicted by *ab initio* calculations[6] and later confirmed.[2] For both isomers, two intermonomer transition frequencies have been observed. One is for an in-plane state and the other for an out-of-plane state.[2,3] Harmonic frequencies have also been computed with *ab initio* methods.[5–7] Although the experimental frequencies for the lower energy C-in isomer are rather close to the *ab initio* harmonic frequencies, the experimental O-in frequencies are not close to the harmonic values. In the C-in

case, the agreement is good enough that the experimental in-plane vibration was assigned to the "CO rock/geared bend." Van der Waals molecules have been avidly studied by experimentalists and theorists for decades.[8–10]

In this paper, we report a new four-dimensional (4D) *ab initio* potential energy surface (PES) that is a function of the intermolecular coordinates of CO–CO$_2$ and energy levels computed on it. The PES is built using points computed at the CCSD(T)-F12b/VTZ-F12 level. The only approximation in the energy-level calculation is the separation of the high frequency intramonomer coordinates from the low frequency intermonomer coordinates. Energy levels and wavefunctions are computed with the Lanczos method and a large spherical-harmonic type basis. It has been demonstrated that such calculations are accurate for other van der Waals dimers.[11–14] Probability Density (PD) and wavefunction cut plots are used to label the energy levels. We find significant coupling between in-plane and out-of-plane coordinates. The experimental transition frequencies are actually from combination bands, but they are expected to be very close to the fundamentals we calculate.
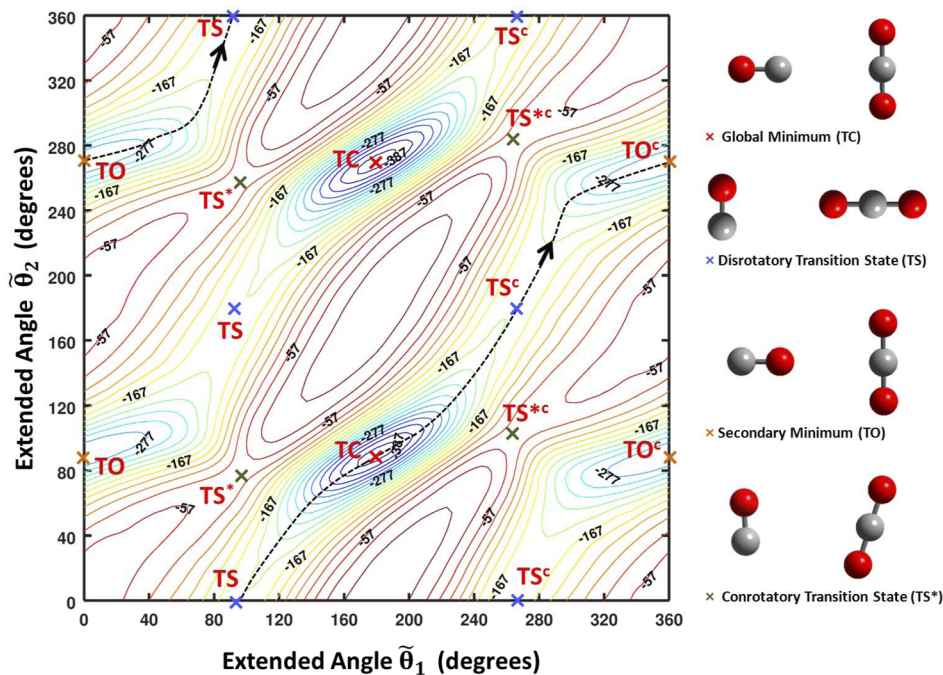
FIG. 1. r_0-optimized contour plot of the PES as a function of the extended angles $\tilde{\theta}_1$ and $\tilde{\theta}_2$. For each pair of angles, the energy (given in cm^{-1}) is optimized with respect to the center-of-mass distance r_0. The position of stationary points—and the corresponding molecular configuration—is highlighted. The extended-angle coordinates are similar to those described elsewhere.[15] Every structure with a c superscript, on the right side, is a copy of a structure on the left side. TS and TS^c label geared transition states; TS* and TS*^{c} are the antigeared transition states. The dashed curve shows the geared path for the molecule, from TC, to TS^c, to TO^c, to TS and back to TC.

II. IMLS PES FITTING

The coordinates used to define the 4D intermolecular CO–CO$_2$ potential, r_0, θ_1, θ_2, and ϕ_2, are depicted in Fig. 2. $\vec{r}_0$ is the vector from the center of mass of CO to the center of mass of CO$_2$; $\vec{r}_1$ and $\vec{r}_2$ are vectors aligned with the monomers. r_0 is the length of $\vec{r}_0$, and θ_1 and θ_2 are (respectively) the angles between $\vec{r}_0$ and the vectors $\vec{r}_1$ and $\vec{r}_2$. The fourth coordinate is the dihedral (out of plane) torsional angle, labeled ϕ_2, which is the angle between the vectors $\vec{r}_0 \times \vec{r}_1$ and $\vec{r}_0 \times \vec{r}_2$.

Both monomers were held rigid. As in previous studies,[15,16] for the CO molecule we used $r_1 = 1.1282$ Å, corresponding to the rotational constant $B = 1.9317$ cm^{-1}.[16,17] CO$_2$ is linear, with each CO bond-distance fixed at $r_{CO} = 1.162\,086$ Å, which is consistent with the experimental rotational constant $0.390\,218\,94$ cm^{-1}.[18,19] Masses of $15.994\,914\,622\,1$ u and 12 u were used for ^{16}O and ^{12}C, respectively. All *ab initio* calculations were performed using the
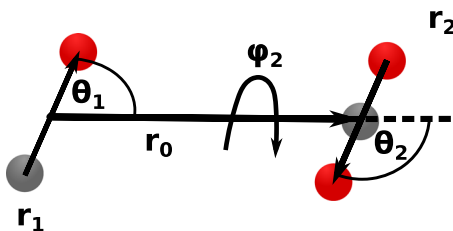
FIG. 2. Coordinates used to describe CO–CO$_2$. r_0: center-of-mass separation (length of $\vec{r}_0$); θ_1, θ_2: angles between $\vec{r}_0$ and the vectors $\vec{r}_1$ and $\vec{r}_2$, respectively, and ϕ_2: torsional angle.
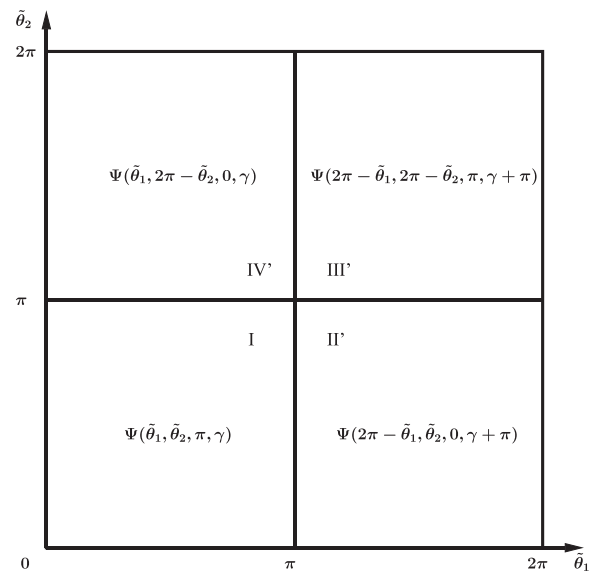
FIG. 3. Definition of the extended angles $(\tilde{\theta}_1, \tilde{\theta}_2)$ in the $[0, 2\pi]$ range. In our convention, monomer 1 is left of monomer 2 and the positive directions for $\tilde{\theta}_1$ and $\tilde{\theta}_2$ are clockwise and counter-clockwise, respectively. Given in each quadrant is the computed wavefunctions $\Psi(\theta_1, \theta_2, \phi_2, \gamma)$. By equating the first (second) argument in Ψ in the figure with $\theta_1(\theta_2)$, one obtains the definition of the extended coordinates in each quadrant. For example, in the bottom right quadrant, $\tilde{\theta}_1 = 2\pi - \theta_1$. The definitions here complement the definitions of the extended angles in the $[-\pi, \pi]$ range given in Ref. 15. Quadrants II′, III′, and IV′′ are obtained from quadrants II, III, and IV of Ref. 15 by shifting one or two angles by 2π.

TABLE I. Equilibrium and transition state geometries and energies for configurations shown in Fig. 1. Absolute energies are relative to the asymptote. θ_1, θ_2, and ϕ_2 are in degrees, and r_0 is in Angström. ϕ_2 for TC and TO is undefined.

Stat. Pt.	$(\theta_1, \theta_2, \phi_2, r_0)$	Ab initio $(\theta_1, \theta_2, \phi_2, r_0)^6$	E_{abs} (cm^{-1})	E_{rel} (cm^{-1})
TC	(180, 90, -, 3.868)	(180, 90, -, 3.957)	−398.3	0
TO	(0, 90, -, 3.534)	(0, 90, -, 3.610)	−297.8	100.43
TS	(90, 180, 0, 4.434)		−180.0	218.3
X	(90, 90, 90, 3.529)		−150.1	248.2
TS*	(92, 76, 0, 6.951)		−97.5	300.8

Molpro electronic structure code package.[20] A lower level guide surface was constructed using data at the explicitly correlated CCSD(T)-F12a/VDZ-F12 level.[21] Data for the final high-level PES were generated using the CCSD(T)-F12b/VTZ-F12 method and basis set.[22]

The 4D PES was constructed using an automated interpolating moving least squares method, which has been used in several previous studies[15,23–25] and has been recently released as a software package under the name AUTOSURF.[26,27] This interpolative approach can accommodate arbitrary energy-surface topographies and is particularly advantageous in cases with large anisotropy, which are challenging for traditional Legendre expansions. The shortest intermonomer center-of-mass distance considered is $R = 2.1$ Å, with the additional restriction of a maximum repulsive energy of 6 kcal/mol ($\sim$2100 cm^{-1}) above the separated monomers' asymptote. To guide the placement of high-level data—and avoid computing and discarding computationally expensive *ab initio* energies in highly repulsive regions—an initial lower-level guide surface was constructed using a set of 1949 symmetry-unique points, distributed using a Sobol sequence biased to sample the short range region more densely. For the high-level PES, the global estimated root-mean-squared fitting error tolerance was set to 0.2 cm^{-1} and the total number of automatically generated symmetry-unique points needed to reach that target was 2654. The *ab initio* data coverage of the fitted PES extends to $R = 20.0$ Å. A local fit was expanded about each data point, and for each of the local fits, a fitting basis of 301 functions was used. The final potential is obtained as the normalized weighted sum of the local fits.

Figure 1 shows the PES in planar configurations. The plot is made by finding the value of r_0 that minimizes the energy for each θ_1, θ_2 pair. The plot is in the extended coordinates, $(\tilde{\theta}_1, \tilde{\theta}_2)$. We use extended coordinates similar to those defined in Ref. 15. They are not identical because we want the range of $(\tilde{\theta}_1, \tilde{\theta}_2)$ to be from 0 to 2π so that wavefunctions on extended plots appear in the middle, and not at the edges. The extended coordinates
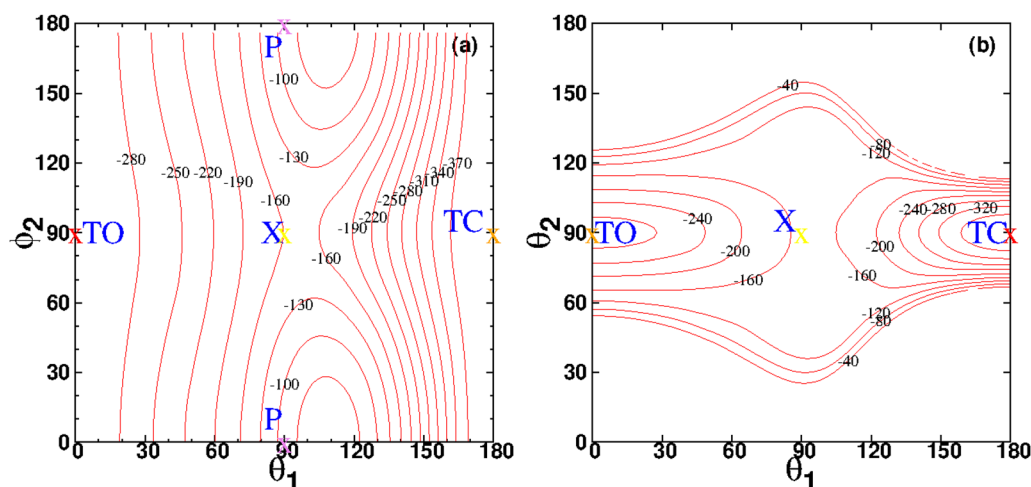

FIG. 4. Two plots showing the out-of-plane path connecting the two isomers. (a) PES as a function of θ_1 and ϕ_2, with $\theta_2 = 90°$, and r_0 equal the value that minimizes the energy, but with the restriction that r_0 must be between the equilibrium values for the isomers. X labels a shape where both isomers form a "cross" shape, and P labels a configuration in which both isomers are in the same plane and parallel to each other with $\theta_1 = \theta_2 = 90°$. Due to the symmetry of CO_2, the value of the potential is identical at ϕ_2 and $360° - \phi_2$ and only the symmetrically unique part of the PES is shown. ϕ_2 is undefined at TC and TO, but when $\theta_1 = 180° - \varepsilon$, or ε where ε is some small angle, the shape of the molecule is almost the same for all ϕ_2 values and TO and TC labels could therefore be put anywhere along the ϕ_2 axis. We put the labels near the ends of the path at about $\phi_2 = 90°$. (b) PES as a function of θ_1 and θ_2, with $\phi_2 = 90°$, and r_0 equal the value that minimizes the energy, with the restriction that r_0 must be between the equilibrium values for both isomers.
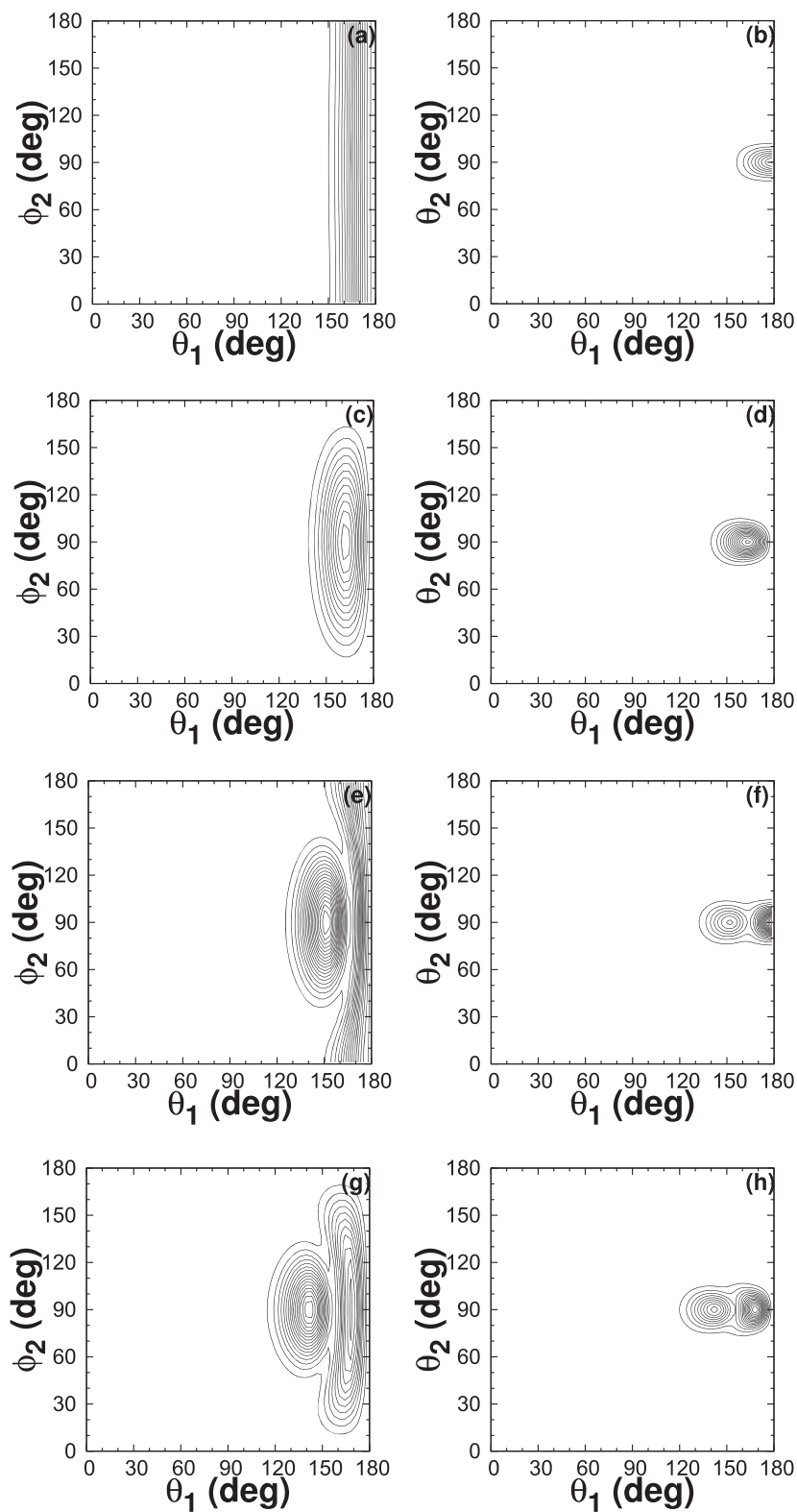
FIG. 5. Probability density plots for the ground state and the first three CO libration states (1B−, 5A+, and 6B−) whose energies are 0.0000, 44.5664, 86.0042, and 123.3091 cm^{-1}, from top to bottom. The left column shows PD plots that are functions of θ_1 and ϕ_2, whereas the right column shows PD plots that are functions of θ_1 and θ_2.

are also used to make wavefunction plots. They are defined in Fig. 3.

The advantage of using extended coordinates is that it is easy to visualize a planar motion during which ϕ_2 changes from $0°$ to $180°$. For example, TC (the global minimum), TS^c, TO^c, TO, and TS are points on a disrotatory (or geared) cycle. The corresponding geared coordinate is $Q_g = \theta_1 + \theta_2$. The path is easily identified in extended coordinates, but one must exit the plot on the right at TO^c and re-enter on the left at TO and also exit at TS at the top of the plot and re-enter at TS at the bottom of the plot. If extended coordinates were not used then to trace this path, one would need to exit and re-enter at the middle of the plot. A disadvantage of using extended coordinates is that every point on the actual PES appears twice in Fig. 1. Not counting copies, there are two minima: labeled "TC" (T-shaped C-in) and "TO" (T-shaped O-in) in the plot; and two saddle points: labeled TS* and TS. Note that the top half of Fig. 1 is equivalent to the bottom half because of the symmetry of CO_2. The minima of the C-in and O-in wells are at -398.273 cm^{-1} and -297.843 cm^{-1}, respectively, both with respect to the dissociation energy of the complex. Geared and antigeared cycles are prominent on the PESs of many dimers.[24,25,28,29] However, the cycle is different in the CO–CO_2 case because the minima are not slipped parallel but T-shaped. The geometries and energies relative to the dissociation energy of the minima are given in Table I.

Venayagamoorthy and Ford reported that the energy difference between the two minima is 99.65 cm^{-1}, whereas our difference is 100.43 cm^{-1}. The TS saddle point is 218.3 cm^{-1} higher than TC. The states we can label (*vide infra*) are all localized in either the O-in well or the C-in well. Because the TS* saddle point is 300.8 cm^{-1} higher than TC, the antigeared path has no influence on the low-lying levels.

There is also an out-of-plane path between TC and TO. It is evident in Fig. 4(a), which shows the PES as a function of θ_1 and ϕ_2, with θ_2 fixed at its value at the bottom of the C-in well and r_0 minimized, but restricted to be between the equilibrium values for both isomers. There is clearly a low-lying path along $\phi_2 = 90°$ from $\theta_1 = \varepsilon$ to $\theta_1 = 180° - \varepsilon$, where ε is some small value. At $\theta_1 = 180°$ and $\theta_1 = 0°$, ϕ_2 is undefined. As θ_1 approaches $180°$ and $0°$, the PES becomes independent of ϕ_2 and it is therefore easy to slip into an out-of-plane configuration from a T-shaped geometry. The saddle point of this path is 248.2 cm^{-1} above TC. The same path is evident in Fig. 4(b), which shows the PES as a function of θ_1 and θ_2 with ϕ_2 fixed at 90 and r_0 minimized, but restricted to be between the equilibrium values for both isomers. As that figure shows, when $\phi_2 = 90°$ there is little coupling between θ_1 and θ_2. When $\phi_2 = 0°$, θ_1 and θ_2 are strongly coupled and the natural motion is along the geared and antigeared ($Q_a = \theta_1 - \theta_2$) coordinates (see Fig. 1). When the two monomers are in the same plane,

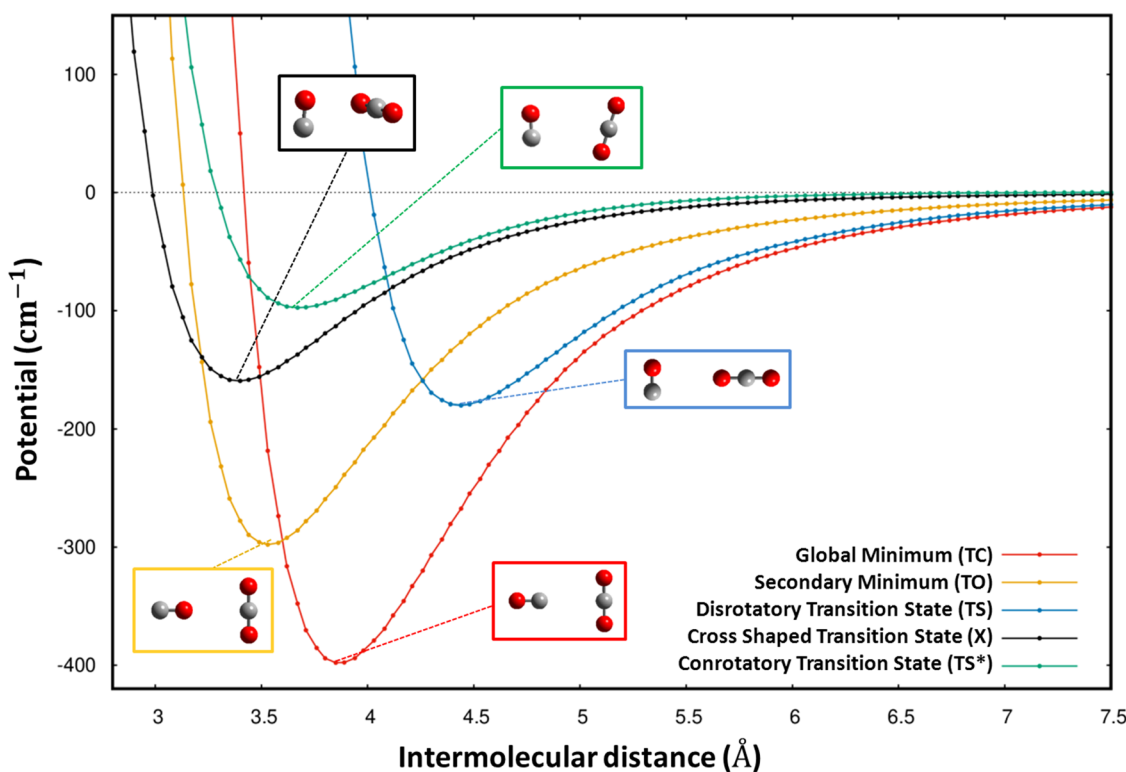**FIG. 6**. Radial cuts through the PES for the stationary points labeled in Fig. 1.

Legend:
- Global Minimum (TC)
- Secondary Minimum (TO)
- Disrotatory Transition State (TS)
- Cross Shaped Transition State (X)
- Conrotatory Transition State (TS*)

θ_1 and θ_2 are coupled because the monomers push against each other. When the two monomers are not in the same plane, θ_1 and θ_2 are not coupled because the monomers do not obstruct each other. Such an out-of-plane path between T-shaped minima might also be important for other van der Waals molecules. In CO–CO$_2$, the fact that ϕ_2 is very floppy manifests itself in the wavefunctions, see Fig. 5.

Figure 6 shows the potential as a function of r_0 upon approach toward each of the stationary points highlighted in Fig. 1. The variation in those cuts gives some indication of the anisotropy of the interactions. To ensure correct symmetry properties, the representation of the PES was symmetrized to provide numerically exact permutation symmetry with respect to exchange of the two O-atoms in CO$_2$. On the quadrature grid, the largest difference between potential values that should be identical is 0.0077 cm^{-1}.

III. SOLVING THE VIBRATIONAL SCHRÖDINGER EQUATION

We solve the Schrödinger equation retaining only the four intermonomer coordinates by using a rovibrational basis and the Lanczos method.[28,30–37] The kinetic energy operator in the Jacobi coordinates of Fig. 2 is well known.[35,38,39] For the rotational constants of CO and CO$_2$, we use 1.922 512 5 cm^{-1} and 0.390 218 94 cm^{-1}, respectively.[25,40]

We represent the Hamiltonian operator in a basis and compute eigenvalues. The basis functions used are

$$f_{a_0}(r_0)u_{l_1 l_2 m_2 K}^{IMP}(\theta_1,\theta_2,\phi_2;\alpha,\beta,\gamma), \qquad (1)$$

where f_{a_0} is a discrete variable representation (DVR) function[41] and $u_{l_1 l_2 m_2 K}^{IMP}$ is a parity adapted rovibrational function.[42,43] α, β, γ are Euler angles, and $P = 0, 1$ correspond to even and odd parities. The DVR we use is a tridiagonal Morse (TDM) DVR.[44] A TDM basis has three parameters: D_e, ω, and r_e. The value of D_e is the value obtained from the cut of the PES with θ_1, θ_2, and ϕ_2 fixed at their values at the bottom of the C-in well. To determine ω and r_e, we choose values that give energy levels less than 140 cm^{-1} that are all within 0.0001 cm^{-1} of the levels obtained with a large sine DVR basis. ω and r_e are varied manually close to the values obtained from the cut used to choose D_e. The sine DVR basis is defined in the range (5.0 bohr and 38.0 bohr) and has 150 functions. The levels below 140 cm^{-1} above the zero point energy (ZPE) computed with the sine DVR basis have convergence errors smaller than 0.0001 cm^{-1}. The final r_0 basis has 20 tridiagonal Morse DVR functions with the parameters $D_e = 398$ cm^{-1}, $\omega = 54.5$ cm^{-1}, and $r_e = 6.85$ bohr. We use[44] $\alpha = A - 2[A/2] = 0.606$, with $A = 4D_e/\omega_e$, in the associated Laguerre polynomial so that all the bound states of the Morse Hamiltonian are exactly reproduced by the TDM basis. $u_{l_1 l_2 m_2 K}^{IMP}$ are parity-adapted combinations of products of Wigner rotation functions, an associated Legendre function, and a spherical harmonic. They have amplitude everywhere in the angular configuration space and allow one to study large amplitude motion. For the angular basis, we used $l_{max} = m_{max} = 45$. The $J = 0$ A+ basis has about 329 000 functions.

Energy levels are calculated with the Lanczos algorithm[45–47] using the RV4 code.[33] The full permutation-inversion (PI) group[48]

is G_4. It has four irreducible representations: A+, A−, B+, and B−, where A/B label states that are symmetric/antisymmetric under permutation of the two O atoms in CO$_2$, and ± label even/odd parity levels. The basis of Eq. (1) can be A/B symmetry-adapted by restricting l_2 to be even/odd, respectively. We therefore separately compute levels within each of the four G_4 symmetry blocks. To evaluate the matrix-vector products, sums are done sequentially.[41] Matrix elements of the kinetic energy operator are exact.[33,35] Potential matrix elements are written as sums over quadrature points.[41,49] We use $N_{\theta_1} = N_{\theta_2} = 46$ Gauss-Legendre quadrature points and $N_{\phi_2} = 92$ equally spaced trapezoid points in the range

TABLE II. Energy levels for both the C-in and O-in isomers. Energies in parentheses are with respect to the O-in isomer's ground state energy. The number in front of the symmetry label is a cardinal number. A 2 before the quantum numbers indicates that the state is localized above the O-in well. v_g, v_a, v_t, and v_s represent the geared, antigeared, CO libration, and stretch quantum numbers, respectively. All energies are with respect to the ZPE, −286.90 cm^{-1}. The ZPE of the C-in isomer is 111.383 cm^{-1} higher than the global minima, TC in Fig. 1.

| E (E_{O-in}) (cm^{-1})	n-sym	(v_g, v_a, v_t, v_s)
0.0000	1A+	(0, 0, 0, 0)
24.4546	1B+	(1, 0, 0, 0)
44.5664	1B−	(0, 0, 1, 0)
47.3698	2A+	(2, 0, 0, 0)
50.2140	3A+	(0,0,0,1)
64.4973 (0.0000)	4A+	2(0, 0, 0, 0)
68.2473	1A−	(1, 0, 1, 0)
68.8211	2B+	(3, 0, 0, 0)
70.0601	3B+	(1, 0, 0, 1)
79.1763 (14.6790)	4B+	2(1, 0, 0, 0)
86.0042	5A+	(0, 0, 2, 0)
87.9203	6A+	(4, 0, 0, 0)
88.6163 (24.12)	2B−	2(0, 0, 1, 0)
89.5665	5B+	(0, 1, 0, 0)
90.2245	3B−	(2, 0, 1, 0)
90.7751	7A+	(2, 0, 0, 1)
92.3644	4B−	(0, 0, 1, 1)
94.1768 (29.6795)	8A+	2(2, 0, 0, 0)
96.2892	9A+	(0, 0, 0, 2)
104.5450 (40.0477)	2A−	2(1, 0, 1, 0)
104.9504	6B+	(5, 0, 0, 0)
107.7748 (43.2775)	10A+	2(0, 0, 0, 1)
107.9768	7B+	
109.7627	3A−	(3, 0, 1, 0)
110.1747 (45.6774)	8B+	2(3, 0, 0, 0)
110.6554	9B+	
111.7702	4A−	
112.9367	10B+	(1, 0, 0, 2)
113.3010 (48.8039)	11B+	2(0, 1, 0, 0)
114.0523 (49.5550)	11A+	2(0, 0, 2, 0)
114.2612	12A+	
119.8673	13A+	
120.6303 (56.1330)	5B−	
123.3091	6B−	(0, 0, 3, 0)
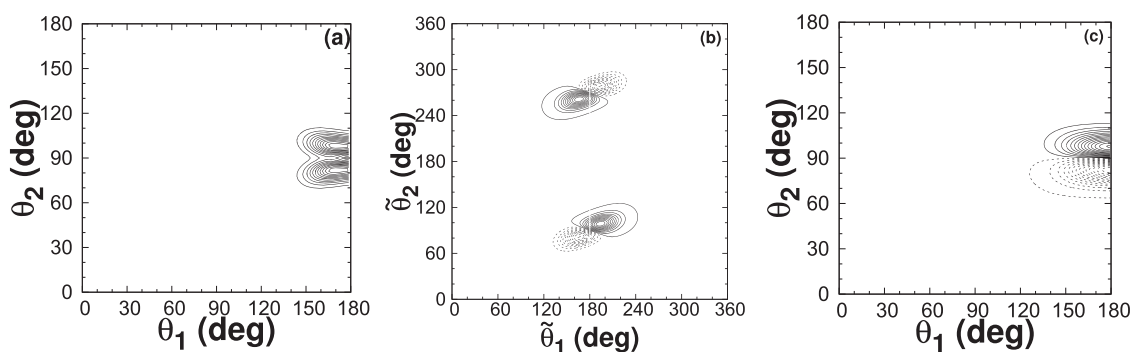
FIG. 7. Plots for the first geared state of the C-in isomer at 24.4546 cm^{-1} (*B+*). (a) Probability density as a function of θ_1 and θ_2, (b) extended wavefunction cut as a function of $\tilde{\theta}_1$ and $\tilde{\theta}_2$, and (c) wavefunction cut as a function of θ_1 and θ_2 at $\phi_2 = 90°$.

[0, 2π]. To reduce the spectral range of the Hamiltonian matrix (and accelerate Lanczos convergence), we use a potential ceiling[49] of $V_{ceil} = 2098.4$ cm^{-1}.

IV. RESULTS

Vibrational levels for both O-in and C-in isomers are listed in Table II with their respective quantum numbers as well as their symmetries. Energies are given with respect to the ZPE and, for states localized in the O-in well, we give in parentheses energies with respect to the ZPE of the lowest level localized in the O-in well. The energies in parentheses can be directly compared with experimental transition frequencies for the O-in isomer. One important result is that the O-in ground state is 64.4973 cm^{-1} higher than the C-in ground state, although the O-in isomer well is 100.5 cm^{-1} higher than the C-in isomer, as shown in Fig. 1. This is due to the fact that the ZPE of the C-in isomer is larger than the ZPE of the O-in isomer. Antigeared vibrational states have higher energies than their geared counterparts (24.4546 and 89.5665 cm^{-1} for the first geared and antigeared states for the C-in isomer, respectively) because the wells are steeper in the antigeared direction.

To make the vibrational assignments presented in Table II, we use 1D and 2D probability distribution (PD) and wavefunction plots. To make a 2D (1D) PD plot, we integrate over the remaining 2 (3) coordinates. From the PD plots (not shown), it is clear that for the low-lying states, coupling between the stretch and other coordinates is weak. Our basic tool for making assignments is the nodal structure of wavefunction plots since they provide more information than PDs. PDs are less useful because a PD includes contributions from sums of squares of wavefunctions for *all* values of the other coordinates. For example, on the basis of the (θ_1, θ_2) PD plot in Fig. 7(a) [Fig. 8(a)] for the geared (antigeared) bending state at 24.4546 cm^{-1} (89.5665 cm^{-1}), one might conclude that θ_1 and θ_2 are weakly coupled (the contour lines are parallel to the axes), but wavefunction cuts in Fig. 7(b) [Fig. 8(b)] reveal that at $\phi_2 = 0°$ and $\phi_2 = 180°$, the vibration occurs along the geared (antigeared) coordinate. Figures 7(c) and 8(c) show that when $\phi_2 = 90°$ the character of the vibrations changes so that in both cases vibration now occurs along θ_2, this means that there is important coupling between ϕ_2 and (θ_1, θ_2).

To assign overtones and combinations, we use not only the nodal structure of wavefunction plots but also the energies of the fundamentals, e.g., once a fundamental is assigned, we look for
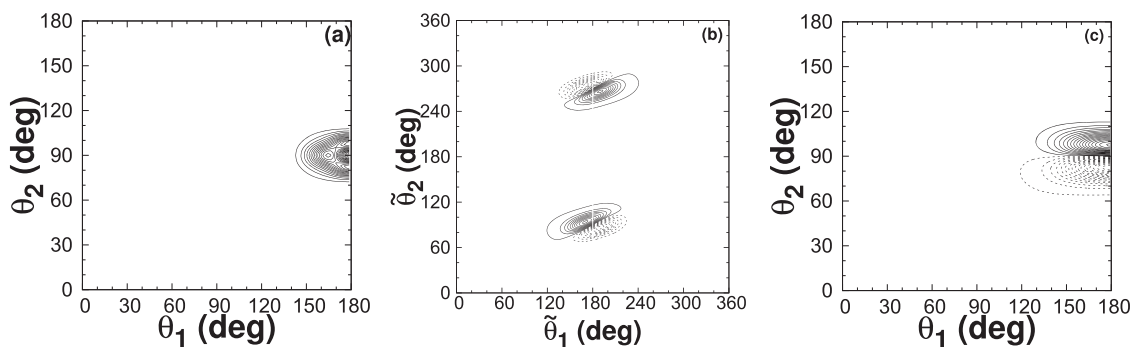

FIG. 8. Probability density plot (a), extended wavefunction cut (b), and wavefunction cut at $\phi_2 = 90°$ (c) for the first antigeared state of the C-in isomer, with energy of 89.5665 cm^{-1} (*5B+*).
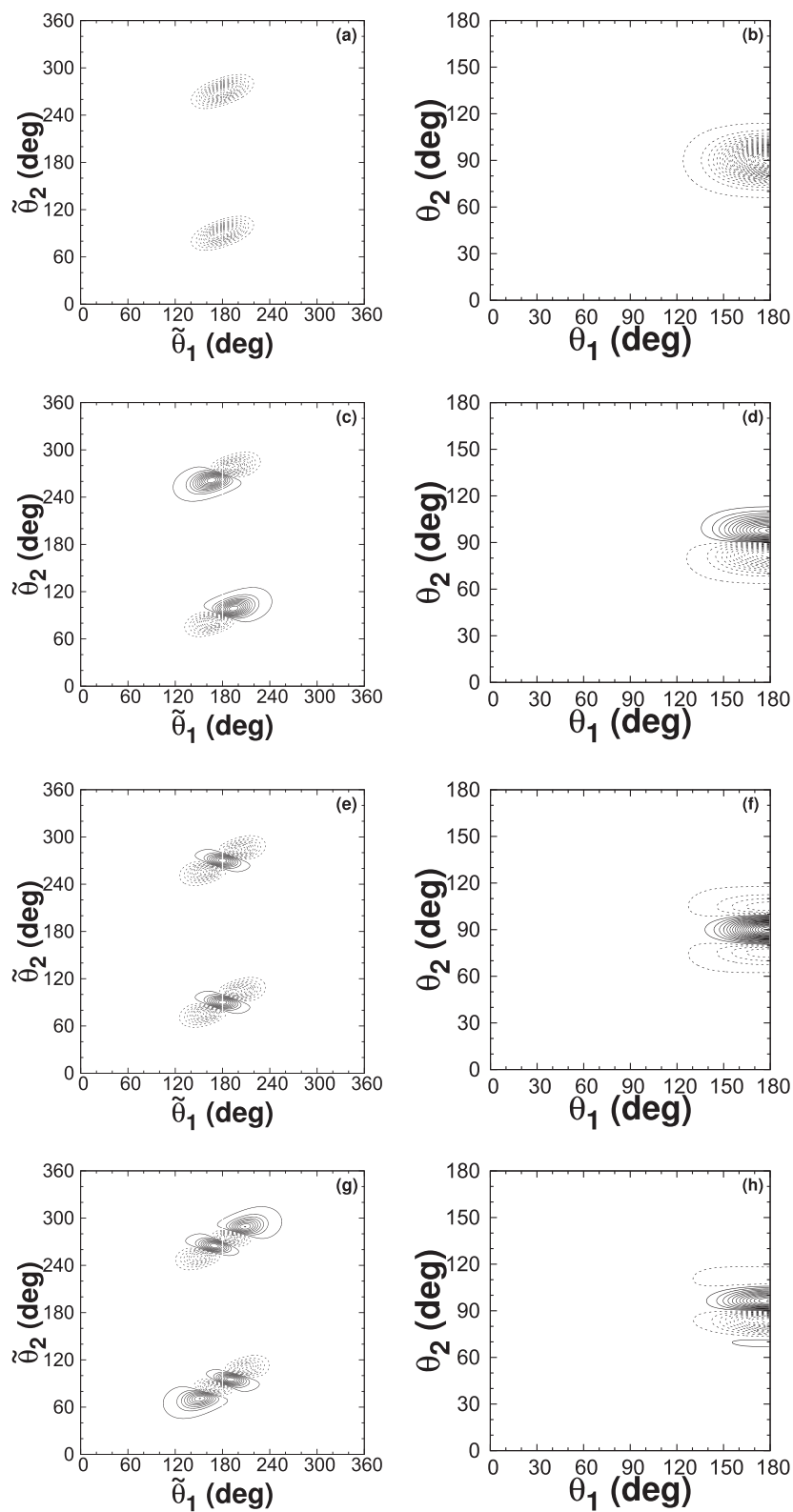
FIG. 9. Wavefunction cuts for the ground state [(a) and (b)] and the first 3 geared states [(c) and (d); (e) and (f); and (g) and (h)] for the C-in isomer whose energies are 0.0000(1A+), 24.4546(1B+), 47.3698(2A+), and 68.8211(2B+) cm^{-1}. The wavefunction cuts on the left are in extended coordinates and show the in-plane behavior of the molecule (both $\phi_2 = 0°$ and $\phi_2 = 180°$); the plots on the right are with $\phi_2 = 90°$. All plots have a fixed value of $r = 7.31$ bohr, the equilibrium value for the C-in isomer. The contour interval for the $\phi_2 = 90$ wavefunction cuts is about half the interval used in the extended plots, in order to show the θ_2 nodal structure more clearly.

TABLE III. Calculated and observed fundamental frequencies, in cm^{-1}.

Sym	State	C-in isomer			O-in isomer		
		Variational	Harmonic[6]	Observed[3]	Variational	Harmonic[6]	Observed[3]
B+	v_g	24.4546	24.30	24.343	14.6790	15.45	14.194
	v_a	89.5665	90.79		45.6774	51.62	
B−	v_t	44.5664	42.81	43.958	24.1190	36.32	22.676
A+	v_s	50.2140	56.39		43.2775	55.37	

TABLE IV. $J = 1$ rotational levels and rotational constants (in cm^{-1}) of the C-in isomer of CO–CO$_2$ for the fundamental vibrational states. Energies are relative to the ZPE of the C-in isomer.

$J = 0$ level (v_g, v_a, v_t, v_s)	1_{01} (sym)	1_{11} (sym)	1_{10} (sym)	A	B	C
0.0000 (0, 0, 0, 0) (A+)	0.1165(A−)	0.4495(B−)	0.4584(B+)	0.3957	0.0627	0.0538
24.4546 (1, 0, 0, 0) (B+)	24.5719(B−)	24.9044(A−)	24.9141(A+)	0.3960	0.0635	0.0538
44.5663 (0, 0, 1, 0) (B−)	44.6838(B+)	45.0166(A+)	45.0250(A−)	0.3957	0.0630	0.0545
50.2140 (0, 0, 0, 1) (A+)	50.3267(A−)	50.6631(B−)	50.6717(B+)	0.3971	0.0606	0.0521
89.5665 (0, 1, 0, 0) (B+)	89.6798(B−)	89.9900(A−)	89.9984(A+)	0.3711	0.0609	0.0525

its overtone near the energy that is about twice the energy of the fundamental. Finally, to confirm assignments we also use symmetry by using product rules for the group C$_{2v}$, e.g., if a state is labeled $v_g + v_t$, its symmetry should be the product of both symmetries, B+ and B−, so this combination state should have an A− symmetry.

Figures 7(b) and 7(c) [Figs. 8(b) and 8(c)] show that although the $\phi_2 = 180°$ wavefunction cut of the state we call the geared

(antigeared) fundamental has a node along the geared (antigeared) coordinate, the $\phi_2 = 90°$ wavefunction cut has nodes along θ_2. A sequence of such geared states is shown in Fig. 9. On the left, it is easy to recognize nodes along the geared coordinate; on the right, the same states have nodes along θ_2. In van der Waals dimers, geared states are very common (see, for example, Ref. 23), but this is the first time that geared states have been seen to change their character when ϕ_2 is changed from 0° or 180° to 90°.

TABLE V. $J = 1$ rotational levels and rotational constants (in cm^{-1}) of the O-in isomer of CO–CO$_2$ for the fundamental vibrational states. Energies are relative to the ZPE of the O-in isomer.

$J = 0$ level (v_g, v_a, v_t, v_s)	1_{01} (sym)	1_{11} (sym)	1_{10} (sym)	A	B	C
0.0000 (0, 0, 0, 0) (A+)	0.1374(A−)	0.4593(B−)	0.4719(B+)	0.3969	0.0750	0.0624
14.6790 (1, 0, 0, 0) (B+)	14.8185(B−)	15.1059(A−)	15.1197(A+)	0.3640	0.0767	0.0629
24.1190 (0, 0, 1, 0) (B−)	24.258(B+)	24.6124(A+)	24.6234(A−)	0.4297	0.0753	0.0637
43.2775 (0, 0, 0, 1) (A+)	43.4130(A−)	43.7998(B−)	43.8117(B+)	0.4605	0.0737	0.0618
48.8038 (0, 1, 0, 0) (B+)	48.9381(B−)	49.2716(A−)	49.2896(A+)	0.4096	0.0761	0.0581

TABLE VI. Rotational constants for the ground, first geared, and CO-libration states of the C-in isomer. All values are in cm^{-1}. Experimental values were obtained by Barclay et al.[3]

	Ground state		v_g		v_t		
	Variational	Expt.	Variational	Expt.	Variational	Expt.	Ab initio Equib.[6]
A	0.3957	0.3957	0.3960	0.3949	0.3957	0.3966	0.3850
B	0.0627	0.0628	0.0635	0.0633	0.0630	0.0629	0.0608
C	0.0538	0.0538	0.0538	0.0537	0.0545	0.0544	0.0525

TABLE VII. Rotational constants for the ground, first geared, and CO-libration states of the O-in isomer. All values are in cm^{-1}. Experimental values were obtained by Sheybani-Deloui et al.[2]

	Ground state		v_g		v_t		
	Variational	Expt.	Variational	Expt.	Variational	Expt.	*Ab initio* Equib.[6]
A	0.3969	0.3972	0.3640	0.3589	0.4297	0.4355	0.3850
B	0.0750	0.0745	0.0767	0.0762	0.0753	0.0749	0.0727
C	0.0624	0.0621	0.0629	0.0626	0.0637	0.0634	0.0612

Figure 5 shows PD plots for CO-libration states. They have nodes along θ_1. The amplitude of the motion along ϕ_2 is clearly large. The O-in isomer has a similar set of states. As a function of ϕ_2, the PD is largest close to $\phi_2 = 90°$. This CO bending therefore occurs when the two monomers are in a cross configuration.

In Table III, we compare the measured intermolecular frequencies we calculate with those obtained by Ford and co-workers.[6] The harmonic frequency for the B− vibration of the O-in isomer is the furthest from the experimental value. The fully coupled result is much closer. It is sometimes the case that higher wells are shallower and less harmonic. In previous papers,[2,3] the B+ state is referred to as in-plane rock. In Table III, it is labeled v_g, where g represents geared. Recall that wavefunction plots reveal that this state is geared when $\phi_2 = 180°$ but a CO$_2$ rock when $\phi_2 = 90°$.

We have computed $J = 1$ energy levels and they are reported, with assignments, in Tables IV and V. There are three closely spaced $J = 1$ levels associated with each vibrational state. Knowing that the molecule is close to a prolate top, we assign the three levels assuming that $1_{01} < 1_{11} < 1_{10}$. Rotational constants are then obtained from the relations $1_{01} = B + C$, $1_{11} = A + C$, and $1_{10} = A + B$. The rotational constants obtained from both isomer's ground states are compared to previous experimental and *ab initio* results in Tables VI and VII, and as it can be seen our constants agree well with previous experiments. The rotational constants obtained by assuming the molecule is rigid are much farther from the experimental values.

V. CONCLUSION

An accurate PES has been constructed and used to compute the low-lying energy levels of CO–CO$_2$. Energy levels were computed using a large spherical harmonic type basis and the Lanczos algorithm. Agreement with experimental band centers and rotation constants is excellent for both isomers. Using PD and wavefunction plots, energy spacing, and symmetry labels, it is possible to assign many states. We are able to confirm that the experimental frequency at 24.3 cm^{-1} is the geared fundamental. Referring to it as geared is, however, a bit of an oversimplification because although it is clearly geared when $\phi_2 = 0°$, it is better described as a CO$_2$ rock when $\phi_2 = 90°$. Additionally, the CO libration was correctly identified and labeled for both isomers.

We have found three low-lying paths between the two isomers. They will influence the dynamics of higher states. One of the three paths is geared. It plays a role for many van der Waals dimers. The second path is antigeared. The third path is out-of-plane. Although

TC is planar, any small change in θ_1 puts the molecule into a region of the PES in which it is almost independent of ϕ_2. Near $\phi_2 = 90°$, it is feasible to change θ_1 to convert the molecule from TC to TO. This may be a common isomerization path between T-shaped isomers.

REFERENCES

[1] A. C. Legon and A. P. Suckley, J. Chem. Phys. **91**, 4440 (1989).

[2] S. Sheybani-Deloui, A. J. Barclay, K. H. Michaelian, A. R. W. McKellar, and N. Moazzen-Ahmadi, J. Chem. Phys. **143**, 121101 (2015).

[3] A. J. Barclay, S. Sheybani-Deloui, K. H. Michaelian, A. R. McKellar, and N. Moazzen-Ahmadi, Chem. Phys. Lett. **651**, 62 (2016).

[4] R. W. Randall, J. P. L. Summersgill, and B. J. Howard, J. Chem. Soc., Faraday Trans. **86**, 1943 (1990).

[5] V. Kellö, K. P. Lawley, and G. H. Diercksen, Chem. Phys. Lett. **319**, 231 (2000).

[6] M. Venayagamoorthy and T. A. Ford, J. Mol. Struct. **565-566**, 399 (2001).

[7] K. M. de Lange and J. R. Lane, J. Chem. Phys. **134**, 034301 (2011).

[8] D. J. Nesbitt, Chem. Rev. **88**, 843 (1988).

[9] Z. Bačić and R. E. Miller, J. Phys. Chem. **100**, 12945 (1996).

[10] D. H. Zhang, Q. Wu, J. Z. Zhang, M. Von Dirke, and Z. Bačić, J. Chem. Phys. **102**, 2315 (1995).

[11] M. Dehghany, M. Rezaei, N. Moazzen-Ahmadi, A. McKellar, J. Brown, X.-G. Wang, and T. Carrington, J. Mol. Spectrosc. **330**, 188 (2016).

[12] X.-G. Wang and T. Carrington, J. Chem. Phys. **143**, 024303 (2015).

[13] H. Cybulski, C. Henriksen, R. Dawes, X.-G. Wang, N. Bora, G. Avila, T. Carrington, and B. Fernández, Phys. Chem. Chem. Phys. **20**, 12624 (2018).

[14] A. J. Barclay, A. R. W. McKellar, N. Moazzen-Ahmadi, R. Dawes, X.-G. Wang, and T. Carrington, Phys. Chem. Chem. Phys. **20**, 14431 (2018).

[15] R. Dawes, X.-G. Wang, and T. Carrington, J. Phys. Chem. A **117**, 7612 (2013).

[16] G. W. M. Vissers, A. Hebelmann, G. Jansen, P. E. S. Wormer, and A. van der Avoird, J. Chem. Phys. **122**, 054306 (2005).

[17] L. A. Surin, D. N. Fourzikov, T. F. Giesen, S. Schlemmer, G. Winnewisser, V. A. Panfilov, B. S. Dumesh, G. W. M. Vissers, and A. van der Avoird, J. Phys. Chem. A **111**, 12238 (2007).

[18] H. Li, P.-N. Roy, and R. J. Le Roy, J. Chem. Phys. **132**, 214309 (2010).

[19] G. Guelachvili, J. Mol. Spectrosc. **79**, 72 (1980).

[20] H.-J. Werner, P. J. Knowles, G. Knizia, F. R. Manby, and M. Schütz, Wiley Interdiscip. Rev.: Comput. Mol. Sci. **2**, 242 (2012).

[21] H.-J. Werner, G. Knizia, and F. R. Manby, Mol. Phys. **109**, 407 (2011).

[22] K. A. Peterson, T. B. Adler, and H.-J. Werner, J. Chem. Phys. **128**, 084102 (2008).

[23] G. Donoghue, X. G. Wang, R. Dawes, and T. Carrington, J. Mol. Spectrosc. **330**, 170 (2016).

[24] X.-G. Wang, T. Carrington, and R. Dawes, J. Mol. Spectrosc. **330**, 179 (2016).

[25] J. Brown, X.-G. Wang, T. Carrington, G. S. Grubbs, and R. Dawes, J. Chem. Phys. **140**, 114303 (2014).

[26] R. Dawes and E. Quintas-Sánchez, *Reviews in Computational Chemistry* (John Wiley & Sons, Inc., 2018), Vol. 31, Chap. 5, pp. 199–264.

[27] E. Quintas-Sánchez and R. Dawes, J. Chem. Inf. Model. **59**, 262 (2019).

[28] J. Brown, X. G. Wang, R. Dawes, and T. Carrington, J. Chem. Phys. **136**, 134306 (2012).

[29] X.-G. Wang, T. Carrington, R. Dawes, and A. W. Jasper, J. Mol. Spectrosc. **268**, 53 (2011).

[30] V. Babin, C. Leforestier, and F. Paesani, J. Chem. Theory Comput. **9**, 5395 (2013).

[31] C. Leforestier, L. B. Braly, K. Liu, M. J. Elrod, and R. J. Saykally, J. Chem. Phys. **106**, 8527 (1997).

[32] C. Leforestier, J. Chem. Phys. **94**, 6388 (1991).

[33] R. Dawes, X. G. Wang, A. W. Jasper, and T. Carrington, J. Chem. Phys. **133**, 134304 (2010).

[34] P. Sarkar, N. Poulin, and T. Carrington, J. Chem. Phys. **110**, 10269 (1999).

[35] X.-G. Wang, T. Carrington, J. Tang, and A. R. W. McKellar, J. Chem. Phys. **123**, 034301 (2005).

[36] S. Y. Lin and H. Guo, J. Chem. Phys. **119**, 5867 (2003).

[37] H. G. Yu, H. Song, and M. Yang, J. Chem. Phys. **146**, 224307 (2017).

[38] G. Brocks, A. van der Avoird, B. Sutcliffe, and J. Tennyson, Mol. Phys. **50**, 1025 (1983).

[39] X. Chapuisat and C. Iung, Phys. Rev. A **45**, 6217 (1992).

[40] R. A. Toth, J. Opt. Soc. Am. B **4**, 357 (1987).

[41] J. C. Light and T. Carrington, Adv. Chem. Phys. **114**, 263 (2000).

[42] X.-G. Wang and T. Carrington, J. Chem. Phys. **121**, 2937 (2004).

[43] X.-G. Wang and T. Carrington, J. Chem. Phys. **118**, 6946 (2003).

[44] H. Wei and T. Carrington, J. Chem. Phys. **97**, 3029 (1992).

[45] X.-G. Wang and T. Carrington, J. Chem. Phys. **115**, 9781 (2001).

[46] X.-G. Wang and T. Carrington, J. Chem. Phys. **114**, 1473 (2001).

[47] R. Chen and H. Guo, J. Chem. Phys. **114**, 1467 (2001).

[48] P. R. Bunker, P. Jensen, and National Research Council Canada, *Molecular Symmetry and Spectroscopy* (NRC Research Press, 1998).

[49] M. J. Bramley, J. W. Tromp, T. Carrington, and G. C. Corey, J. Chem. Phys. **100**, 6175 (1994).